Topology-Controlled Microphase Separation and Interconversion of Twist and Writhe Domains in Supercoiled Annealed Polyelectrolytes

Roman Staňo,[1,2,*] Christos N. Likos,[1] Davide Michieletto,[3,4] and Jan Smrek[1]
[1]Faculty of Physics, University of Vienna, Boltzmanngasse 5, 1090 Vienna, Austria
[2]Yusuf Hamied Department of Chemistry, University of Cambridge, Lensfield Road, Cambridge CB2 1EW, United Kingdom
[3]School of Physics and Astronomy, University of Edinburgh, Peter Guthrie Tait Road, Edinburgh EH9 3FD, United Kingdom
[4]MRC Human Genetics Unit, Institute of Genetics and Cancer, University of Edinburgh, Edinburgh EH4 2XU, United Kingdom

(Received 14 November 2024; revised 16 June 2025; accepted 30 June 2025; published 23 July 2025)

In closed circular ribbonlike polymers such as deoxyribonucleic acid, twist and writhe are known to be largely determined by the polymer's bending and torsional rigidities, and they must sum to a topological constant. Using molecular simulations and an analytically solvable Landau theory, we study the interplay between ribbon topology and chemically annealed charges in a model polyelectrolyte. We show that the repulsions between like-charged acidic sites trigger phase separation and coexistence of supercoiling domains, in turn unveiling a complex phase diagram and providing a route to control the properties of deoxyribonucleic acid-based materials.

DOI: 10.1103/7fh5-frst

Deoxyribonucleic acid (DNA) is ubiquitous in living organisms and now commonly used in smart materials [1–5]. Most exisiting DNA nanotechnology is based on Watson-Crick base pairing [6–8]; however, leveraging DNA topology [9] to guide material design is less common. Circular DNA carries topological invariants that strongly impact its conformations and physical properties [10,11], e.g., a linear DNA can relax torsional stress through the free ends while a ring DNA, or plasmid, cannot. Indeed, the topology of circular DNA and other ribbonlike closed curves must obey the White-Fuller-Călugăreanu theorem (WFC) [12], stating that the twist Tw (the winding of the two edges of the ribbon) and the writhe Wr (the winding of the curve centerline with itself) must sum to a constant [13], i.e., $\mathrm{Tw} + \mathrm{Wr} = \mathrm{Lk}$, where Lk is the linking number. The degree of supercoiling can be defined as $\sigma = (\mathrm{Lk} - \mathrm{Lk}_0)/\mathrm{Lk}_0$, where Lk_0 is the linking number between the two ribbon edges (or DNA strands) in the thermodynamically relaxed state [9,14]. This conservation law entails that closed circular DNA can interconvert twist into writhe, generating so-called plectonemic conformations [9,15–20]. The interplay between twist and writhe affects dynamic, thermodynamic, and entanglement features [21,22] and can also influence the viscoelastic properties of dense solutions of plasmids [23].

*Contact author: roman.stano@univie.ac.at

In circular DNA, the partitioning of supercoiling into twist and writhe is thermodynamically determined by the ratio of the torsional and bending constants [24,25]. In isolated and equilibrated DNA plasmids, the partitioning of Lk in twist and writhe is uniform along the whole closed molecule, and there are no methods to control interconversion and partitioning of writhe or twist reversibly [9,26–28].

In this Letter, we propose a novel method to dynamically control the balance of twist and writhe by contrasting the bending-torsion competition with long-ranged electrostatic repulsion. Since electrostatic repulsion disfavors writhe-rich conformations—as they display numerous intrachain contacts—writhe is thermodynamically converted into twist at large enough repulsion, which is here tuned via the solution pH. Employing annealed charges to control repulsion is commonly used to destabilize supramolecular assemblies and gels [29–31], and it has been proposed as a possible mechanism to localize and tie knots on diblock copolymers [31]. However, it has never been considered to tune the supercoiling in ribbonlike structures.

Achieving dynamic control over twist-writhe interconversion and their partition is a promising avenue to tune the mechanical properties of such materials and complex fluids, e.g., polyelectrolytes [23], graphene nanoribbons [32], biological fibers [33,34], catenanes [35–37], circular helicenes [38], and other ribbonlike molecules [39–43].

Simulation model and method—We consider a single unknotted ring polymer (Fig. 1) represented as a twistable elastic chain of $N = 200$ repulsive monomeric units connected by finitely extensible springs [44] (see Supplemental Material [45] and Ref. [46] for more details). Each monomeric unit is a rigid body formed by a central

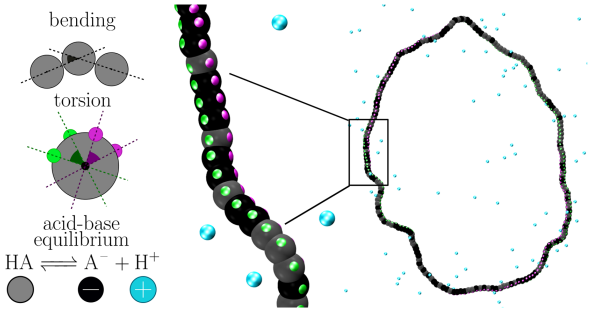

FIG. 1. Left: schematic depiction of three key components of polymer bending, torsion, and pH-controlled chemical equilibrium. Right: snapshot of a twist-rich ring polymer with $\sigma = 1\%$ at $\Delta\mathrm{pH} = 5$ with the inset showing a detail of the patches inscribing orientation into the monomeric units.

Weeks-Chandler-Andersen spherical particle with three patches that do not interact sterically, but set the monomers' orientation. The latter is used in modeling torsion between consecutive pairs of monomeric units using a dihedral potential, controlling the preferred pitch along the chain $p = 2\pi/\psi_0$, where ψ_0 is the angle for which the dihedral potential has the minimum. By choosing appropriate ψ_0 (the same for all the bonds), we can control the total degree of supercoiling $\sigma = |\mathrm{Lk}|/N$, where Lk is the linking number defined as $\mathrm{Lk} = N/p$ and is a measure of the total torsional-bending stress contained within the polymer [23]. Bending between consecutive triplets of central beads is constrained by a Kratky-Porod potential with resulting persistence length of $l_p \approx 25b$, where b is the mean bond length. The parameters of the potentials mimic those of double-stranded DNA, but our results are generalizable to other polymers.

The central bead of each monomeric unit is modeled as a weak acid, which can participate in chemical reaction equilibrium $\mathrm{HA} \rightleftharpoons \mathrm{A}^- + \mathrm{H}^+$, and exists in either charged (A^-) or uncharged (HA) state with charge number $Q = -1$ or $Q = 0$, respectively. The system also contains explicit counterions with excluded volume and charge number $Q = +1$ in such amount so that the overall charge of the system is zero. The charged moieties interact via the Coulomb potential $U = k_\mathrm{B}T l_\mathrm{B} Q_i Q_j / r$, where $l_\mathrm{B} = e^2/(4\pi\varepsilon_0\varepsilon_r k_\mathrm{B}T)$ is the Bjerrum length. The electrostatic interactions are evaluated using the P3M method [47] with relative accuracy 10^{-3} and $l_\mathrm{B} \approx b$, roughly corresponding to the critical Manning charge density [63–65] chosen to prevent the counterion condensation.

To sample the configurations and equilibrium charge states of the model, we use molecular dynamics with a Langevin thermostat combined with stochastic Monte Carlo charge-regulation moves [48]. This algorithm randomly changes the charge state of the monomeric units in accordance with an acceptance probability that depends on energy and chemical potentials from the reaction balance. The algorithm emulates chemical equilibrium of the acidic groups at a chosen input $\Delta\mathrm{pH} = \mathrm{pH} - \mathrm{p}K_\mathrm{A}$, where pH controls the chemical potential of H^+ ions and $\mathrm{p}K_\mathrm{A} = 6.0$ is the reaction equilibrium constant, chosen arbitrarily but within typical range of weak acids, as detailed in the Supplemental Material [45]. The system contains no salt or other counterions.

Low supercoiling—First, we focus on flat ribbons with $\sigma = 0\%$. The amount of mean charge on a monomeric unit monotonically increases with ΔpH, in a trend similar for all degrees of supercoiling but significantly deviating from the Henderson-Hasselbalch equation, valid for the noninteracting system, Fig. 2(a). Within the explored range, at a given ΔpH the interacting system is charged less, in comparison to the ideal system. As we increase ΔpH and with it the amount of charge on the polymer, it becomes progressively harder to charge up more of the units because of the repulsive interactions between the like-charged monomeric units on the polymer contour, posing an excess free energy penalty for charging, coined as the polyelectrolyte effect [49,50,66,67]. To overcome the penalty, one has to impose higher chemical potential by increasing ΔpH, resulting in a shift of the ionization response to higher values of ΔpH as compared to the ideal case.

Accumulation of the charge on the polymer contour causes conformational changes shown in Fig. 2(b). By increasing ΔpH, the ring swells to mitigate the strong repulsions between like-charged monomeric units, resulting in almost 30% increase of minimal surface area and radius of gyration in the limit of maximal charging ($\Delta\mathrm{pH} = 5$), as compared to the limit of the uncharged ring ($\Delta\mathrm{pH} = -1$). Concomitantly, the average shape of rings changes from spherical into more disklike (Fig. S3 in Supplemental Material [45]). Finally, for the flat ribbon, $\sigma = 0\%$, and as Fig. 2(c) shows, both twist and writhe of the ribbon are zero in the whole range of the ΔpH values, as increasing either of them would increase bending or torsional energy, respectively.

Next, we focus on the case of low but nonzero supercoiling $\sigma = 1\%$. In the limit of the uncharged polymer, the resultant conformations on Fig. 2(d) are rather compact [Fig. 2(b)] and writhe-dominated [Fig. 2(c)], resulting in almost zero twist. Nevertheless, high writhe inevitably entails abundant close contacts between monomeric units; increasing ΔpH and associated charging disfavors such structures, promoting swelling and separation between the charged monomers. Since increasing monomer separation and swelling necessarily reduces the overall writhe (self-entanglement) of the polymer to conserve the global Lk, the polymer must increase its twist, as seen in Fig. 2(c). Eventually, this leads to fully swollen disklike twist-dominated conformations Fig. 2(d). The minimal surface area of the ring due to pH sweep in the full range of charging increases more than three times, underlining the potential of this mechanism to control the conformation of ribbonlike polymers in solution. The transition

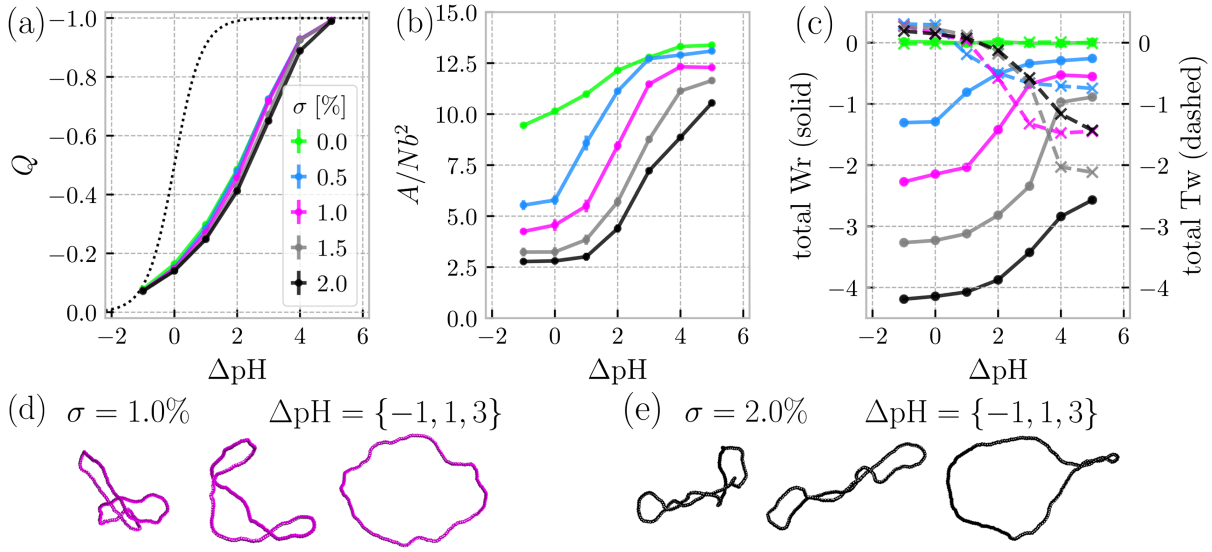

FIG. 2. Global properties of the system for different degrees of supercoiling σ. (a) Mean charge on a monomeric unit as a function of pH. The dotted line corresponds to the noninteracting system. (b) Area of the minimal surface spanned on the ring as a function of pH, showing conformational opening upon charging. (c) Total writhe and total twist of the polymer as a function of pH, showing topological changes upon charging. (d),(e) Representative snapshots of ring conformations at low and high supercoiling, respectively, for selected pH values covering the whole range of possible charge states.

from plectonemic (writhe-rich) to swollen (twist-rich) is smooth and does not show signs of a sharp first-order phase transition.

High supercoiling—In the limit of high supercoiling $\sigma \gtrsim 2.0\%$, uncharged rings ($\Delta\mathrm{pH} = -1$) are dominated by writhe and exhibit tight supercoiled conformations [Fig. 2(e)], with available surface area significantly smaller than their low supercoiling counterparts. These configurations are reminiscent of double-folded ring polymers, which can be observed in melts [51,68]; nevertheless, the double-folded conformations of our polymer with $N = 200$ are linearlike, as opposed to branched trees, observed in melts of long rings ($N \gtrsim 800$). When increasing ΔpH, the polymer contour charges up, the conformation remains tight, but the double-folded chain straightens up, becoming rodlike due to electrostatic persistence, known from conventional polyelectrolyte theories [69]. Only at $\Delta\mathrm{pH} \gtrsim 1$, we observe larger conformational changes, namely loosening of the double-folded conformation and creation of swollen loops, which concentrate charges and, by swelling, facilitate mitigation of electrostatic repulsions, as shown in Fig. 2(e). This conformational change is accompanied by loss of writhe at the expense of gained twist [Fig. 2(c)]. Ultimately, at $\Delta\mathrm{pH} \gtrsim 3$, the charged loops fuse into a highly swollen, twist-dominated and higher-than-average charged region, which coexists with a writhe-dominated, lower-than-average charged subchain. In Fig. 3, we show the local writhe, local twist, and local charge profiles along a representative molecule. From this figure it is clear that the local topology of the molecule (writhe- or twist-rich domains) is linked to the local charging in those segments. Indeed, the segments with local writhe close to zero exhibit charge density above average, while segments with nonzero writhe have charge density below average. This is an example of a topologically constrained microphase separation, where writhe-dominated and twist-dominated domains coexist along the same molecule. To our knowledge, this type of domain formation has neither been predicted nor observed for isolated ribbonlike polyelectrolytes in solution.

Landau theory—To rationalize the observed microphase coexistence and transition from writhe-dominated to twist-dominated conformations, we model the system using a phenomenological Landau-like mean field theory. Guided by the underlying symmetries of the system, we write the free energy in the form $F = a_0\phi^2 + a_1\phi^4 + a_2(w - w_0)^2 + a_3(w - w_0)^4 + \chi w^2\phi^2 - \mu\phi$, where the order parameter ϕ represents the charge density, μ is the corresponding chemical potential (a proxy of ΔpH), and w is the writhe density—a nonconserved order parameter capturing the supercoiling conformational features. Note that we chose to model the writhe field w, which thus need not be conserved, as opposite to the linking number field (see End Matter for details). The coupling between the charge and the conformation is governed by the parameter $\chi > 0$ and the squares of both, w and ϕ, because our model does not distinguish between left- and right-handed torsion as well as the sign of the charge. At zero coupling, the free energy is minimized at $w = w_0$ (a proxy for σ) that reflects the initial supercoiling degree at zero charge density. We note that our free energy resembles the one successfully employed to describe the melting of torsionally constrained DNA [21], with the difference that here we model the

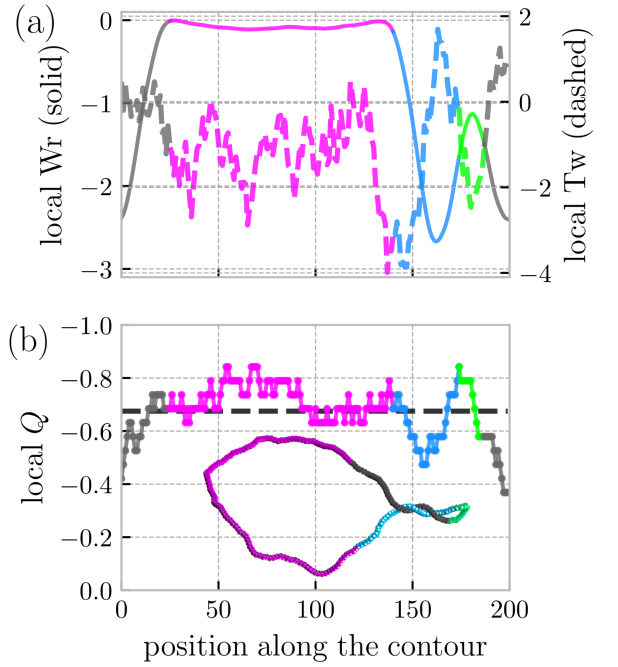

FIG. 3. Relation between local geometry and local charging for a single ring configuration at $\sigma = 2\%$ and $\Delta\text{pH} = 3$. (a) Local writhe (solid) and local twist (dashed) on a monomer, for all the monomers along the contour. (b) Local mean charge on the monomers along the contour with the dashed black line corresponding to the mean charge averaged over the whole ring. To suppress noise, all of the local quantities for a monomer are averaged over the probe monomers and its five neighboring units in both directions along the contour. The color coding corresponds to specific parts of the contour as shown on the inset snapshot.

writhe field (instead of the supercoiling field) and the charge field (instead of the denaturation field).

In Fig. 4, we show various representations of the phase diagram resulting from the free energy for $\mu > 0$, corresponding to the chosen charge sign. For definitiveness, we set all parameters a_0, a_1, a_2, a_3 to unity, while the coupling parameter χ is set to $\chi = 100$. The qualitative features of the phase diagram are not sensitive to these choices provided all the parameters are positive (as they should be to capture some basic physical ingredients such as to favor $w = w_0$ with no charge and $\phi = 0$, and to disfavor higher supercoiling at nonzero charge). For given μ and w_0, minimization of the free energy F with respect to ϕ results in a single minimum at $\phi(w, \mu) > 0$ [see Fig. 4(b)]. Note that the monotonic $\phi(w, \mu)$ is independent of w_0, showing, however, that one requires higher μ to charge a system with higher w (see Supplemental Material [45], Fig. S8), in agreement with our simulations, Fig. 2(a). Inserting the equilibrium $\phi(w, \mu)$ back into the Landau expression, we study the resulting free energy profile $F(w, w_0, \mu)$. At low supercoiling w_0, the free energy has a *single* minimum, which for low charge is located close to $w = w_0$ and progressively deepens and shifts toward $w = 0$ (zero writhe) as μ is increased (points A–C in Fig. 4). This transition agrees with our observations for low supercoiling, shown in Fig. 2(d). As ΔpH is increased, writhe-dominated conformations transform into twist-dominated swollen conformations with zero writhe overall.

At high supercoiling the free energy has a more complex behavior. At low charge there is still just a single minimum close to $w = w_0$, but as μ (or ΔpH) is increased, we observe that F develops a second, higher, local minimum closer to $w = 0$, which progressively deepens and starts to dominate

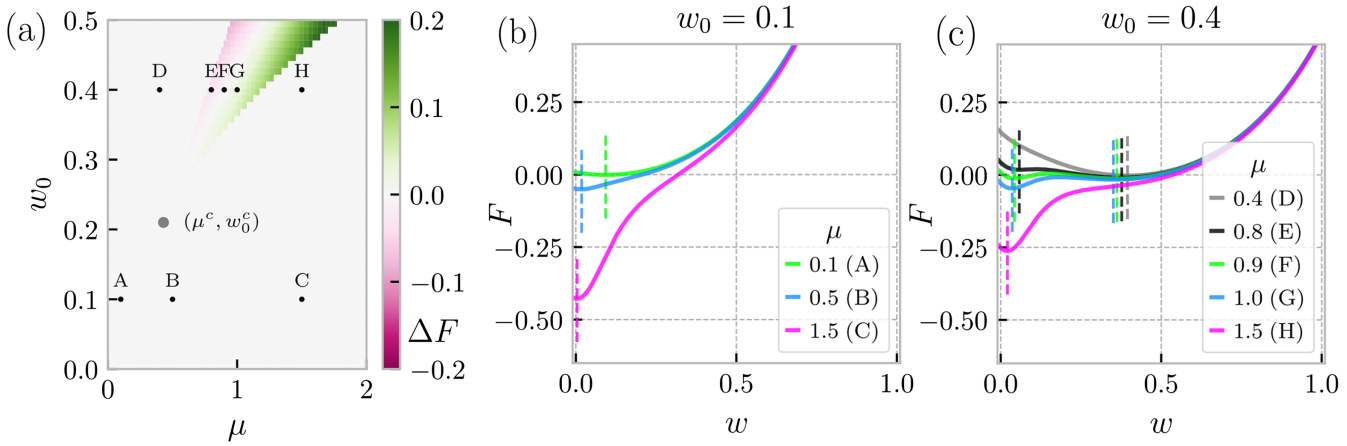

FIG. 4. Describing the conformational transitions using the Landau theory. (a) The phase diagram on the pH-supercoiling plane, using the chemical potential μ and the supercoiling parameter w_0 as coordinates. The colored domain corresponds to the two-phase region with color corresponding to the free energy difference between the two solutions (see color bar on the right), and the large gray dot denotes the critical point. (b) Free energy profiles (solid) after substitution of the $\phi(w, \mu)$ value obtained by minimizing F with respect to ϕ as a function of writhe for the low supercoiling case, and for the three selected points from (a). Dashed lines mark the free energy minima. (c) Same as panel (b) for the high supercoiling case, for five selected points from panel (a).

as the original minimum vanishes. This behavior is characteristic of a first-order, abrupt phase transition, as the system switches from one minimum to another. We also find a line of equal depth minima in the $w_0 - \mu$ plane that ends at a critical point (at about $w_0^c = 0.21$, $\mu^c = 0.43$) exhibiting a second-order conformational phase transition.

Despite the fact that F displays a first-order behavior, we should note that, in practice, the writhe field is constrained by the WFC theorem. This gives rise to the topologically controlled microphase separation that we observed in simulations. Close to the first-order transition, the free energy becomes concave in a range of writhe w, and the system partitions into domains that are writhe rich and twist rich to globally conserve the linking number (or supercoiling). This phase separation hides the first-order nature of the transition in our simulations [21]. Finally, we have confirmed that the choice of the coupling parameter χ does not alter the topology of the phase diagram. Indeed, there exists a line of critical points $[\mu^c(\chi), w_0^c(\chi)]$ in an extended, three-dimensional phase diagram parameterized by the triplet μ, w_0, and χ.

Conclusions—We have combined computer simulations with a phenomenological Landau theory to examine the intricate interplay between charge density and topological features in supercoiled annealed polyelectrolytes. We have shown that for low degrees of supercoiling, a neutral and writhe-dominated polymer will convert writhe into twist as a result of an increase in the pH. In contrast, for high supercoiling the same mechanism leads to a topologically constrained domain coexistence: an overcharged twist-rich domain coexists with an undercharged writhe-rich one.

Recent progress in synthetic methods enabled preparation of nucleotides *functionalized* by weakly acidic side chains [70]. These nucleotides can be polymerized to linear fragments of superanionic acidic DNA up to several hundreds of base pairs, preserving the secondary and tertiary structure of the DNA. In such derivatives, the DNA essentially provides a scaffold controlled by the WFC theorem, and the charge regulation would take place on the weakly acidic side chains, not directly on the DNA phosphates. While DNA rings with such chemistry have not been synthesized yet, we propose that such macromolecules, created either by polymerization or by functionalization of plasmids, could be excellent candidates to exhibit topology-controlled transitions steered by the charge regulation of the side chains tuned by pH.

The control over electrostatic repulsions can be attained also by adding salt (see Fig. S5 in Supplemental Material [45]). Since swollen circular polymers have, at infinite dilution, significantly different rheological response to shear and elongational flow than double-folded, thin ones [71–75], we argue that our findings may be experimentally verifiable using functionalized supercoiled DNA rings in microfluidic channels with buffers with controllable pH or, alternatively, with optical tweezers in the presence of intercalating dyes [76,77]. For concentrated systems, the electrostatic interactions will be screened to some degree, depending on concentration. Our additional simulations employing screened Coulomb interactions (see Supplemental Material [45]) demonstrate that the key features of the phenomena presented in this Letter remain unaffected albeit weakened quantitatively by the effect of salt. Moreover, recent findings regarding charged, stiff ring polymers at high concentrations [78] show that charged minirings organize in stacks of oblate, open conformations penetrated by "needles" of prolate ones. A likely scenario for concentrated solutions of ribbonlike polymers is, thus, the emergence of twist-rich domains that would again self-organize into stacks, whereas a minority of rings could remain writhe rich and thread through these stacks in the region populated by the counterions, which provide strong screening and, therefore, favor writhed configurations.

Acknowledgments—R. S. acknowledges the financial support by the Doctoral College Advanced Functional Materials-Hierarchical Design of Hybrid Systems DOC 85 doc.funds funded by the Austrian Science Fund (FWF) [grant DOI: 10.55776/P35891]. R. S. is funded by the UK Research and Innovation (UKRI) Engineering and Physical Sciences Research Council (EPSRC) under the UK Government's guarantee scheme (EP/Z002028/1), following funding by the European Research Council (Consolidator Grant) under the European Union's Horizon Europe research and innovation programme. This work was supported by a Short-Term Scientific Mission Grant from COST Action CA17139 [79] funded by COST [80]. The computational results presented have been achieved using the Vienna Scientific Cluster (VSC). R. S. thanks C. A. Brackley and Y. A. G. Fosado for technical support and assistance with some of the calculations. D. M. acknowledges the Royal Society and the European Research Council (Grant No. 947918, TAP) for funding.

[1] C. A. Mirkin, R. L. Letsinger, R. C. Mucic, and J. J. Storhoff, A DNA-based method for rationally assembling nanoparticles into macroscopic materials, Nature (London) **382**, 607 (1996).

[2] S. Biffi, R. Cerbino, F. Bomboi, E. M. Paraboschi, R. Asselta, F. Sciortino, and T. Bellini, Phase behavior and critical activated dynamics of limited-valence DNA nanostars, Proc. Natl. Acad. Sci. U.S.A. **110**, 15633 (2013).

[3] M. Panoukidou, S. Weir, V. Sorichetti, Y. G. Fosado, M. Lenz, and D. Michieletto, Runaway transition in irreversible polymer condensation with cyclization, Phys. Rev. Res. **6**, 023189 (2024).

[4] D. Michieletto, P. Neill, S. Weir, D. Evans, N. Crist, V. A. Martinez, and R. M. Robertson-Anderson, Topological digestion drives time-varying rheology of entangled DNA fluids, Nat. Commun. **13**, 4389 (2022).

[5] M. E. Leunissen, R. Dreyfus, R. Sha, T. Wang, N. C. Seeman, D. J. Pine, and P. M. Chaikin, Towards self-replicating materials of DNA-functionalized colloids, Soft Matter **5**, 2422 (2009).
[6] N. C. Seeman and H. F. Sleiman, DNA nanotechnology, Nat. Rev. Mater. **3**, 17068 (2017).
[7] P. W. K. Rothemund, Folding DNA to create nanoscale shapes and patterns, Nature (London) **440**, 297 (2006).
[8] E. Stiakakis, N. Jung, N. Adžić, T. Balandin, E. Kentzinger, U. Rücker, R. Biehl, J. K. G. Dhont, U. Jonas, and C. N. Likos, Self assembling cluster crystals from DNA based dendritic nanostructures, Nat. Commun. **12**, 7167 (2021).
[9] A. Bates and A. Maxwell, *DNA Topology*, Oxford Bioscience (Oxford University Press, New York, 2005).
[10] L. Tubiana *et al.*, Topology in soft and biological matter, Phys. Rep. **1075**, 1 (2024).
[11] M. Kruteva, J. Allgaier, and D. Richter, Topology matters: Conformation and microscopic dynamics of ring polymers, Macromolecules **56**, 7203 (2023).
[12] G. Călugăreanu, Sur les classes d'isotopie des noeuds tridimensionnels et leurs invariants, Czech. Math. J. **11**, 588 (1961).
[13] F. B. Fuller, The writhing number of a space curve, Proc. Natl. Acad. Sci. U.S.A. **68**, 815 (1971).
[14] K. Klenin and J. Langowski, Computation of writhe in modeling of supercoiled DNA, Biopolymers **54**, 307 (2000).
[15] E. Skoruppa and E. Carlon, Equilibrium fluctuations of DNA plectonemes, Phys. Rev. E **106**, 024412 (2022).
[16] M. Segers, E. Skoruppa, H. Schiessel, and E. Carlon, Statistical mechanics of multiplectoneme phases in DNA, Phys. Rev. E **111**, 044408 (2025).
[17] A. Fathizadeh, H. Schiessel, and M. R. Ejtehadi, Molecular dynamics simulation of supercoiled DNA rings, Macromolecules **48**, 164 (2015).
[18] B. A. Krajina and A. J. Spakowitz, Large-scale conformational transitions in supercoiled DNA revealed by coarse-grained simulation, Biophys. J. **111**, 1339 (2016).
[19] R. N. Irobalieva, J. M. Fogg, D. J. Catanese, T. Sutthibutpong, M. Chen, A. K. Barker, S. J. Ludtke, S. A. Harris, M. F. Schmid, W. Chiu, and L. Zechiedrich, Structural diversity of supercoiled DNA, Nat. Commun. **6**, 8440 (2015).
[20] N. Gilbert and J. Allan, Supercoiling in DNA and chromatin, Curr. Opin. Genet. Dev. **25**, 15 (2014).
[21] Y. A. G. Fosado, D. Michieletto, and D. Marenduzzo, Dynamical scaling and phase coexistence in topologically constrained DNA melting, Phys. Rev. Lett. **119**, 118002 (2017).
[22] Y. A. G. Fosado, D. Michieletto, C. A. Brackley, and D. Marenduzzo, Nonequilibrium dynamics and action at a distance in transcriptionally driven DNA supercoiling, Proc. Natl. Acad. Sci. U.S.A. **118**, e1905215118 (2021).
[23] J. Smrek, J. Garamella, R. Robertson-Anderson, and D. Michieletto, Topological tuning of DNA mobility in entangled solutions of supercoiled plasmids, Sci. Adv. **7**, eabf9260 (2021).
[24] C. R. Calladine, H. Drew, F. B. Luisi, and A. A. Travers, *Understanding DNA: The Molecule and How It Works* (Elsevier Academic Press, New York, 1997).
[25] J. F. Marko and E. D. Siggia, Statistical mechanics of supercoiled DNA, Phys. Rev. E **52**, 2912 (1995).
[26] J. C. Wang, DNA topoisomerases, Annu. Rev. Biochem. **54**, 665 (1985).
[27] Y. Pommier, A. Nussenzweig, S. Takeda, and C. Austin, Human topoisomerases and their roles in genome stability and organization, Nat. Rev. Mol. Cell Biol. **23**, 407 (2022).
[28] K. N. Kreuzer and N. R. Cozzarelli, Formation and resolution of DNA catenanes by DNA gyrase, Cell **20**, 245 (1980).
[29] H. Frisch, J. P. Unsleber, D. Lüdeker, M. Peterlechner, G. Brunklaus, M. Waller, and P. Besenius, pH-switchable ampholytic supramolecular copolymers, Angew. Chem. Int. Ed. **52**, 10097 (2013).
[30] R. Otter and P. Besenius, Supramolecular assembly of functional peptide–polymer conjugates, Org. Biomol. Chem. **17**, 6719 (2019).
[31] A. Tagliabue, C. Micheletti, and M. Mella, Tunable knot segregation in copolyelectrolyte rings carrying a neutral segment, ACS Macro Lett. **10**, 1365 (2021).
[32] A. F. Fonseca, Twisting or untwisting graphene twisted nanoribbons without rotation, Phys. Rev. B **104**, 045401 (2021).
[33] R. E. Goldstein, T. R. Powers, and C. H. Wiggins, Viscous nonlinear dynamics of twist and writhe, Phys. Rev. Lett. **80**, 5232 (1998).
[34] P. E. S. Silva, J. L. Trigueiros, A. C. Trindade, R. Simoes, R. G. Dias, M. H. Godinho, and F. V. de Abreu, Perversions with a twist, Sci. Rep. **6**, 23413 (2016).
[35] J. Liu, M. Wu, L. Wu, Y. Liang, Z.-B. Tang, L. Jiang, L. Bian, K. Liang, X. Zheng, and Z. Liu, Infinite twisted polycatenanes, Angew. Chem. Int. Ed. **62**, e202314481 (2023).
[36] L. F. Hart, J. E. Hertzog, P. M. Rauscher, B. W. Rawe, M. M. Tranquilli, and S. J. Rowan, Material properties and applications of mechanically interlocked polymers, Nat. Rev. Mater. **6**, 508 (2021).
[37] L. Tubiana, F. Ferrari, and E. Orlandini, Circular polycatenanes: Supramolecular structures with topologically tunable properties, Phys. Rev. Lett. **129**, 227801 (2022).
[38] J. Malinčík, S. Gaikwad, J. P. Mora-Fuentes, M.-A. Boillat, A. Prescimone, D. Häussinger, A. G. Campaña, and T. Šolomek, Circularly polarized luminescence in a Möbius helicene carbon nanohoop, Angew. Chem., Int. Ed. **61**, e202208591 (2022).
[39] L. Giomi and L. Mahadevan, Statistical mechanics of developable ribbons, Phys. Rev. Lett. **104**, 238104 (2010).
[40] E. H. Yong, F. Dary, L. Giomi, and L. Mahadevan, Statistics and topology of fluctuating ribbons, Proc. Natl. Acad. Sci. U.S.A. **119**, e2122907119 (2022).
[41] B. Mergell, M. R. Ejtehadi, and R. Everaers, Statistical mechanics of triangulated ribbons, Phys. Rev. E **66**, 011903 (2002).
[42] R. Golestanian and T. B. Liverpool, Statistical mechanics of semiflexible ribbon polymers, Phys. Rev. E **62**, 5488 (2000).
[43] W. Michaels, A. J. Spakowitz, and J. Qin, Conformational statistics of ribbon-like chains, Macromolecules **56**, 8359 (2023).

[44] K. Kremer and G. S. Grest, Dynamics of entangled linear polymer melts: A molecular-dynamics simulation, J. Chem. Phys. **92**, 5057 (1990).
[45] See Supplemental Material at http://link.aps.org/supplemental/10.1103/7fh5-frst for details of the model, methods, and additional results, which include Refs. [14,22,23,46–62].
[46] C. A. Brackley, A. N. Morozov, and D. Marenduzzo, Models for twistable elastic polymers in Brownian dynamics, and their implementation for LAMMPS, J. Chem. Phys. **140**, 135103 (2014).
[47] R. W. Hockney and J. W. Eastwood, *Computer Simulation Using Particles* (IOP, London, 1988).
[48] T. Curk, J. Yuan, and E. Luijten, Accelerated simulation method for charge regulation effects, J. Chem. Phys. **156**, 044122 (2022).
[49] J. Landsgesell, P. Hebbeker, O. Rud, R. Lunkad, P. Košovan, and C. Holm, Grand-reaction method for simulations of ionization equilibria coupled to ion partitioning, Macromolecules **53**, 3007 (2020).
[50] J. Landsgesell, L. Nová, O. Rud, F. Uhlík, D. Sean, P. Hebbeker, C. Holm, and P. Košovan, Simulations of ionization equilibria in weak polyelectrolyte solutions and gels, Soft Matter **15**, 1155 (2019).
[51] J. Smrek, K. Kremer, and A. Rosa, Threading of unconcatenated ring polymers at high concentrations: Double-folded vs time-equilibrated structures, ACS Macro Lett. **8**, 155 (2019).
[52] S. Plimpton, Fast parallel algorithms for short-range molecular dynamics, J. Comput. Phys. **117**, 1 (1995).
[53] W. R. Smith and B. Triska, The reaction ensemble method for the computer simulation of chemical and phase equilibria. I. Theory and basic examples, J. Chem. Phys. **100**, 3019 (1994).
[54] J. K. Johnson, A. Z. Panagiotopoulos, and K. E. Gubbins, Reactive canonical Monte Carlo, Mol. Phys. **81**, 717 (1994).
[55] C. Heath Turner, J. K. Brennan, M. Lísal, W. R. Smith, J. Karl Johnson, and K. E. Gubbins, Simulation of chemical reaction equilibria by the reaction ensemble Monte Carlo method: A review, Mol. Simul. **34**, 119 (2008).
[56] A. Narros, A. J. Moreno, and C. N. Likos, Effects of knots on ring polymers in solvents of varying quality, Macromolecules **46**, 3654 (2013).
[57] R. Staňo, C. N. Likos, and J. Smrek, To thread or not to thread? Effective potentials and threading interactions between asymmetric ring polymers, Soft Matter **19**, 17 (2023).
[58] J. Smrek and A. Y. Grosberg, Minimal surfaces on unconcatenated polymer rings in melt, ACS Macro Lett. **5**, 750 (2016).
[59] K. A. Brakke, The surface evolver, 10.1080/10586458.1992.10504253 (1992).
[60] J. L. Sleiman, R. H. Burton, M. Caraglio, Y. A. Gutierrez Fosado, and D. Michieletto, Geometric predictors of knotted and linked arcs, ACS Polym. Au **2**, 341 (2022).
[61] N. Clauvelin, W. K. Olson, and I. Tobias, Characterization of the geometry and topology of DNA pictured as a discrete collection of atoms, J. Chem. Theory Comput. **8**, 1092 (2012).
[62] D. McQuarrie, *Statistical Mechanics*, Chemistry Series (Harper & Row, New York, 1975).
[63] G. S. Manning, Limiting laws and counterion condensation in polyelectrolyte solutions I. Colligative properties, J. Chem. Phys. **51**, 924 (1969).
[64] A. Naji and R. R. Netz, Scaling and universality in the counterion-condensation transition at charged cylinders, Phys. Rev. E **73**, 056105 (2006).
[65] M. Deserno, C. Holm, and S. May, Fraction of condensed counterions around a charged rod: Comparison of Poisson-Boltzmann theory and computer simulations, Macromolecules **33**, 199 (1999).
[66] A. Katchalsky and J. Gillis, Theory of the potentiometric titration of polymeric acids, Recl. Trav. Chim. Pays-Bas **68**, 879 (1949).
[67] E. Raphael and J.-F. Joanny, Annealed and quenched polyelectrolytes, Europhys. Lett. **13**, 623 (1990).
[68] E. Ghobadpour, M. Kolb, M. R. Ejtehadi, and R. Everaers, Monte Carlo simulation of a lattice model for the dynamics of randomly branching double-folded ring polymers, Phys. Rev. E **104**, 014501 (2021).
[69] J. Skolnick and M. Fixman, Electrostatic persistence length of a wormlike polyelectrolyte, Macromolecules **10**, 944 (1977).
[70] N. Kuprikova, M. Ondruš, L. Bednárová, M. Riopedre-Fernandez, L. P. Slavětínská, V. Sýkorová, and M. Hocek, Superanionic DNA: Enzymatic synthesis of hypermodified DNA bearing four different anionic substituents at all four nucleobases, Nucl. Acids Res. **51**, 11428 (2023).
[71] C. Schneck, J. Smrek, C. N. Likos, and A. Zöttl, Supercoiled ring polymers under shear flow, Nanoscale **16**, 8880 (2024).
[72] M. Liebetreu, M. Ripoll, and C. N. Likos, Trefoil knot hydrodynamic delocalization on sheared ring polymers, ACS Macro Lett. **7**, 447 (2018).
[73] M. Liebetreu and C. N. Likos, Hydrodynamic inflation of ring polymers under shear, Commun. Mater. **1**, 4 (2020).
[74] K.-W. Hsiao, C. M. Schroeder, and C. E. Sing, Ring polymer dynamics are governed by a coupling between architecture and hydrodynamic interactions, Macromolecules **49**, 1961 (2016).
[75] M. Q. Tu, M. Lee, R. M. Robertson-Anderson, and C. M. Schroeder, Direct observation of ring polymer dynamics in the flow-gradient plane of shear flow, Macromolecules **53**, 9406 (2020).
[76] G. A. King, F. Burla, E. J. G. Peterman, and G. J. L. Wuite, Supercoiling DNA optically, Proc. Natl. Acad. Sci. U.S.A. **116**, 26534 (2019).
[77] S. H. Kim, M. Ganji, E. Kim, J. van der Torre, E. Abbondanzieri, and C. Dekker, DNA sequence encodes the position of DNA supercoils, eLife **7**, e36557 (2018).
[78] R. Staňo, J. Smrek, and C. N. Likos, Cluster formation in solutions of polyelectrolyte rings, ACS Nano **17**, 21369 (2023).
[79] https://eutopia.unitn.eu/
[80] https://www.cost.eu

End Matter

Landau theory details—The use of a nonconserved writhe field instead of a linking number field means that in principle the optimal writhe value could then exceed the linking number; this does not happen in practice for the parameter choices at hand, which, therefore, provide a quantitative rationalization of the simulation results. The nonconserved character of w implies that the system chooses the value of the writhe that minimizes its free energy, which is equivalent to saying that the chemical potential corresponding to the writhe vanishes identically, $\mu_w = 0$. Accordingly, there is no $\mu_w w$ term in the Landau free energy, and no common tangent construction can be made between phases of different values of the writhe. Coexistence of two such phases can only occur when two equal minima of F with respect to w occur.